Journal of Engineering and Technological Sciences

Role of Deagglomeration in Particle Size and Antibiofilm Activity of ZnO Nanoparticles Synthesized with Averrhoa bilimbi Extract

Vita Wonoputri¹, Tjokorde Walmiki Samadhi^{1*}, Shafira Khairunnisa² & Eka Rahayu³

¹Faculty of Industrial Technology, Institut Teknologi Bandung, Labtek X Building, Jalan Ganesa 10 Bandung 40132, Indonesia

²Laboratory of Microbiology, Indonesian Food and Drug Authority Regional Office in Bandung, Jalan Pasteur 25 Bandung 40171, Indonesia

³Research Center of Food Technology and Processing, National Research and Innovation Agency, Jalan Jogja-Wonosari Km.31, Gading, Yogyakarta 55861, Indonesia

Abstract

Averrhoa bilimbi fruit extract was utilized as a reducing and capping agent in the biosynthesis of zinc oxide nanoparticles, with an emphasis on the effects of in-situ deagglomeration on physical properties and antibiofilm activity against Escherichia coli. The study explored various biosynthesis parameters, namely deagglomeration method (physical vs chemical), temperature (30, 60 °C), and zinc precursor-to-extract volumetric ratio (0.5 and 2). High purity crystalline ZnO nanoparticles were obtained by calcining biosynthesis precipitates at 375 °C. The resulting particles consisted of the wurtzite ZnO phase, with diameters ranging from 18 to 30 nm. The hydrodynamic mean particle diameters were 1.0 to 3.5 μ m, suggesting the formation of soft agglomerates. Physical deagglomeration was more effective at higher temperatures, while chemical deagglomeration was more efficient at lower temperatures, owing to the interaction between the deagglomeration method and biosynthesis temperature. The biosynthesized ZnO nanoparticles exhibited good antibiofilm activity, achieving a 61% reduction in biofilm population at 50 ppm ZnO, which increased to 78% at a dose of 200 ppm. This activity was improved by lower biosynthesis temperature and precursor:extract ratio, likely due to the preservation of bioactive molecules. The results demonstrate the potential of biosynthesized ZnO nanoparticles as antibiofilm agent, offering enhanced effectiveness compared to commercial ZnO nanoparticles.

Keywords: antibacterial; antibiofilm; biosynthesis; nanoparticle; plant extract; ZnO.

Introduction

Nanoparticle is a general term for a vast array of solid particulate materials with nominal dimensions within the 1-100 nm range. The dimensionality of nanoparticles includes 0D ('dots'), 1D, 2D, and 3D particle geometries [1]. The extremely small particle dimension implies that surface-related forces are dominant. As such, physico-chemical properties – thermal, optical, electrical, magnetic, and catalytic properties – of nanoparticles are generally distinct from those associated with the same solid phases at microscopic and macroscopic dimensions.

Biomedical application of nanomaterials has become a rapidly growing field of research in recent years. Classes of nanomaterials in biomedicine include metals (metallic, bimetallic, metal oxides, and magnetic nanoparticles), fullerenes, polymeric nanoparticles, and dendrimers. Their biomedical applications encompass precision drug delivery, hyperthermia therapy, photoablation therapy, bioimaging assistance and biosensors [2, 3]. Biocompatibility is a fundamental issue in the biomedical application of any nanomaterial. It is defined as the ability of nanomaterials to perform their intended medical therapeutic functions without eliciting unmanageable levels of undesirable local or systemic effects, while generating the most beneficial cellular or tissue response. Biocompatibility of nanoparticles is a complex, case-specific behavior influenced by particle geometry, surface charge, hydrophobicity, solubility, size distribution, agglomeration tendency, and other factors [2, 4].

While various metal-based nanomaterials or nanoparticles have been developed, only a limited number of metal oxide nanoparticles (MONP) are deemed safe for biomedical applications for mammals, namely titanium dioxide (TiO₂), zinc

Copyright ©2024 Published by IRCS - ITB ISSN: 2337-5779

^{*}Corresponding author: twsamadhi@itb.ac.id

oxide (ZnO), copper oxide (CuO₂), ferric oxide (Fe₂O₃), and ferrous oxide (Fe₃O₄) [5]. Among these oxides, ZnO appears to exhibit relatively high biocompatibility. Contact of ZnO with aqueous environment typical of human and animal physiological systems causes the slow release of Zn^{2+} cations, which are naturally present in such systems. Additionally, ZnO in the form of both nanoparticles and bulk materials exhibits biodegradability [6]. As such, among MONPs, only ZnO and Fe₂O₃ are classified as GRAS (generally regarded as safe) by the United States FDA [7].

Zinc oxide (ZnO) as an oxide material in the nanoparticle form has found widespread application due to its advantageous engineering properties. ZnO exists in three crystalline polymorphic structures, namely wurtzite, zincblende, and rocksalt. Of these polymorphrs, wurtzite is in stable form at ambient conditions. ZnO exhibits semiconductivity with an energy band gap of 3.37 eV, providing it with a broad electromagnetic absorption band. Additionally, the noncentrosymmetric wurtzite crystal structure produces pronounced piezoelectric effect [8]. In industrial chemical processes, ZnO is important due to its high chemical stability and photocatalytic activity [9].

The generally good human biocompatibility of ZnO has spurred recent research efforts in its application in medicine and health. These include areas such as therapeutic carriers, biological sensing and labeling, gene transfer, nanomedicine discovery, implant coating, water treatment processes, and more [10]. Studies published in the literature have also identified the antimicrobial properties of ZnO nanoparticles, either applied singularly or in combination with other medicines (e.g. antibiotics). Overall, ZnO nanomaterials are regarded as a particularly useful class of nanomaterials in antimicrobial applications due to their ability to kill and to inhibit bacterial growth [11].

It is generally hypothesized that the antimicrobial activity of ZnO nanoparticles mainly stems from the generation of a variety of reactive oxygen species (ROS), which imposes oxidative stress upon microbial cells [12]. Additionally, Zn²⁺ cations are released by ZnO upon prolonged contact with aqueous environment bonds with proteins, carbohydrates, and other biocomponents associated with bacteria, which disrupt their cellular functions [13]. Zinc cations may also diffuse across the bacterial cell wall and interact with protein functional groups within the intracellular space, resulting in the disruption of enzymatic activities and cellular structural alterations [14]. Bacterial cell walls may also be damaged due to the abrasive nature of ZnO nanoparticles and by the neutralization of lipopolysaccharides electrostatic charge by Zn²⁺ cations in proximity of the cell wall [15]. In addition to these mechanisms, it has also been proposed that near-UV emission caused by sunlight radiation on ZnO nanoparticles may induce a non-contact lethal effectagainst bacteria. This last mechanism has been proposed for ZnO nanoparticles embedded in polymeric films [16]. Figure 1 presents a schematic description of these antibacterial mechanisms.

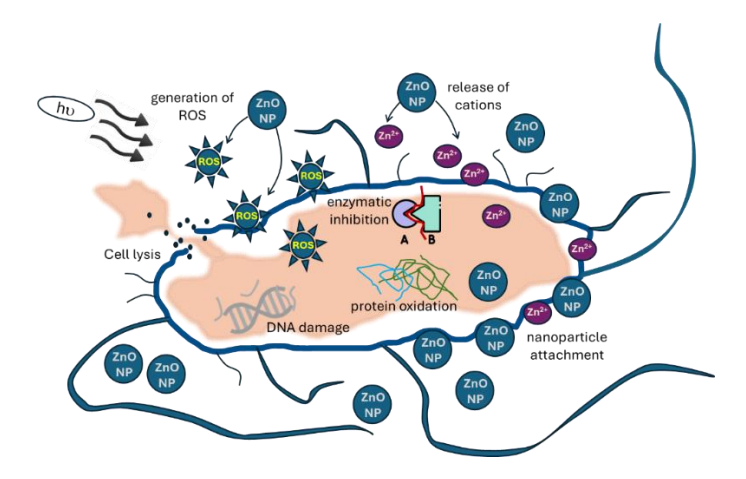


Figure 1 Representative schematic of antibacterial mechanisms of ZnO nanoparticles.

ZnO nanoparticle production pathways can be categorized into physical, chemical, and biological processes. Among them, biological synthesis — also referred to as green synthesis or biosynthesis — is particularly interesting, since it does not employ hazardous chemicals or harsh processing conditions. Biosynthesis assisted by plant extracts basically involves the reduction and precipitation of metal ions from a precursor salt solution by biomolecules in the extracts of various parts of plants such as leaves, bark, fruits, seeds, roots, and tubers. These plant biomolecules also stabilize the formed nanoparticles by acting as capping agents. This plant-extract assisted biosynthesis method has been applied to various metal oxide nanoparticles, such as ZnO, TiO₂, and CuO [17-19]. It has been hypothesized that plant phytochemicals may reduce metallic ions in the aquatic solution phase more rapidly than metabolites produced by

., 0

microbes, which represent a different class of nanoparticle biosynthesis aid agents. Furthermore, plants tend to be non-pathogenic and contain more biomolecules per unit mass [20].

A wide variety of plant extracts have been studied for the biosynthesis of ZnO nanoparticles, mostly focusing on antimicrobial applications. Several review papers have compiled numerous examples of plant extracts used in ZnO biosynthesis [20, 21]. Notably, extracts from plant families such as Myrtaceae, Lauraceae, Plantaginaceae, and Cucurbitaceae have produced nanoparticles with outstanding performance, characterized by low minimum inhibitory concentration (MIC) values and small particle sizes. In contrast, nanoparticles synthesized from extracts of the Apocynaceae and Asphodelaceae plant families tend to exhibit higher MIC values and larger particle sizes [20]. A previous work has identified that the use of bilimbi (*Averrhoa bilimbi*) fruit extract for zinc nanoparticle biosynthesis is technically feasible [18]. This tree plant species, which belongs to the Oxalidaceae family, is commonly found throughout the Southeast Asia region. The fruit has been reported as being rich in antioxidants that are useful in nanoparticle biosynthesis, including phenols, flavonoids, alkaloids, saponins, and tannins [22]. Compared to other fruit species in the region, such as *Averrhoa carambola*, *Capsicum frutescens*, *Canarium sp.*, *Malus domesticus*, and others, total phenolics and the antioxidant content of *A. bilimbi* are moderate [23, 24]. However, this fruit is largely underutilized in the region due to its strongly sour taste [25], which makes its potential use in nanoparticle synthesis particularly interesting.

The abovementioned work and other references have identified the relatively strong agglomeration tendency of biosynthesized zinc nanoparticles. A previous review emphasized the scarcity and controversy associated with agglomeration issue in biosynthesized nanoparticles [26]. Several references argued that certain biomolecules in plant extracts such as phenolic acids from rice husk and sodium lignosulfonate from wood act as dispersants during biosynthesis due to interparticle steric hindrance provided by these biomolecules [27, 28]. In contrast, others contend that the biomolecules actually act as agglomerants due to disruption of the oxide particles' electrical double layer and reduction of system pH by the acidity of the extracts [29-31]. This agglomeration could potentially decrease the antimicrobial activity due to reduction of the available nanoparticle surface area and bacterial contact inhibition [18, 32, 33]. This in turn reduces the amount of Zn²⁺ cations released into the cells to a level that is not sufficiently toxic for the bacteria. Furthermore, large agglomerates may undergo sedimentation, decreasing the concentration of nanoparticles available in the suspended state below the total dose administered to the bacterial system [34]. This shows the need for a deagglomeration strategy for biosynthesized antimicrobial nanoparticles. A physical deagglomeration approach using ultrasonication, which breaks apart agglomerates via induced mechanical vibration, has been argued to be the most effective [35]. Chemical deagglomeration typically involves the addition of dispersants, which increase interparticle repulsive forces and/or steric hindrance. For medicine-oriented antimicrobial applications, these dispersants should preferably be non-toxic [36]. Commonly studied dispersants for ZnO nanoparticles include polyvinyl alchohol (PVA), polyvinyl pyrrolidone (PVP), oleic acid (OA), glycidoxypropyltrimethoxysilane (GPTMS), and others. Overall, PVA tends to produce the highest stability of nanoparticle suspension in water among these chemicals [37, 38].

The current work compared the experimental results obtained using physical and chemical deagglomeration in ZnO nanoparticle biosynthesis aided by bilimbi fruit extract. Key response variables in this work included the nanoparticle size distribution, product phase and morphology, and antimicrobial activity. More specifically, the latter was studied in the context of inhibition of bacterial biofilm, a type of bacterial colony that is more difficult to eradicate.

Materials and Methods

Nanoparticle Biosynthesis

Fresh bilimbi fruits were purchased from a local market in the Bandung municipality, washed by demineralized water and manually pulped using mortar and pestle. The thick pulp was diluted with demineralized water and fed to a three-neck flask at a solid to water ratio of 1:10 (w/v). This mixture was refluxed at 70 °C for 90 minutes. Afterwards the refluxed mixture was collected in the flask, cooled down to room temperature, and filtered using filter paper. The obtained clear bilimbi fruit extract was kept refrigerated at 4 °C and used as stock for the entire experimental work.

ZnO nanoparticle biosynthesis experimentation combined with deagglomeration was undertaken by the 2³ two-level full factorial statistical experiment presented in Table 1. Each experimental run was conducted in triplicate. All statistical analysis of the full factorial experiment was performed using Minitab. For the precursor solution, analytical grade zinc

nitrate (ZnNO₃·6H₂O 98%, Sigma-Aldrich) was dissolved in demineralized water to a concentration of 0.05 M. In the physical deagglomeration pathway, the glass beaker containing the Zn precursor solution was immersed in an ultrasonic water bath and heated at the targeted reaction temperature. The bilimbi fruit extract was subsequently added in a dropwise manner according to the prescribed precursor-to-extract volume ratios. After the fruit extract addition was completed, the mixture was further agitated for 3 hours before letting it cool down. For chemical deagglomeration, the flask containing the reaction mixture was heated on a heating plate. Dropwise addition of bilimbi fruit extract was then done under constant agitation at 500 rpm. Five minutes after the fruit extract addition was completed, 1% PVA solution (prepared by dissolving analytical grade PVA (Merck) in demineralized water) was added at a PVA:Zn precursor solution volume ratio of 1:10. The mixture was then further agitated for 3 hours and cooled down to ambient temperature. The lower biosynthesis temperature in Table 1 represents ambient conditions, while 60 °C is the temperature at which thermal degradation of polyphenols starts to accelerate [39]. The precursor-to-extract volumetric ratios in Table 1 are typical values reported in the literature [40, 41].

Upon completion of the combined biosynthesis-deagglomeration step, the obtained reaction mixture suspension was aged at ambient temperature for 18 hours to increase the amount of precipitated nanoparticles. After aging, the suspension was separated by centrifugation at 10,000 rpm for 15 minutes, followed by washing by demineralized water and re-centrifugation. The supernatant was then carefully removed by pipetting and the precipitate was dried in an oven at 80 °C and calcined to remove residual organic matter and to ensure the formation of crystalline ZnO phase. To determine the appropriate calcination temperature, a precipitate specimen from a preliminary experiment was analyzed by a TGA-DSC apparatus (Linseis STA PT1600, Analytical Instrumentation Laboratory of the Chemical Engineering Department, Institut Teknologi Bandung). The calcined ZnO products were then manually ground and kept in airtight containers.

Francisco contal for atoms	Natation.	Factor to	Values of levels		
Experimental factors	Notation	Factor type	(-1) or low	(+1) or high	
Deagglomeration method	X ₁	Qualitative	Chemical	Physical	
Synthesis temperature (°C)	X_2	Quantitative	30	60	
Precursor:extract (v/v)	X3	Quantitative	1:2	2:1	

Table 1 Notations and levels of ZnO biosynthesis experimental variables.

Physical Characterization of Nanoparticles

The key physical properties of the nanoparticles that were characterized included the identification of crystalline phases, particle size distribution, and particle morphology.

A Bruker D8 X-ray diffraction (XRD) apparatus (Department of Chemical Engineering, Institut Teknologi Bandung) was used to confirm the formation of ZnO. The XRD instrument used a Cu-K α radiation source, with the diffraction angle 20 set at 10-80° range. The nanoparticle specimens selected for XRD were obtained at a zinc precursor:extract ratio of 1:2 and a biosynthesis temperature of 60 °C. The X-ray diffraction pattern of the specimens was compared with the JCPDS No. 00-036-1451 standard diffraction pattern for wurtzite ZnO as the typical dominant phase in ZnO nanoparticles [42]. Commercial ZnO nanoparticles (Sigma Aldrich) were also analyzed as comparison.

Nanoparticle morphology was analyzed using a Hitachi HT-7700 transmission electron microscope (TEM) instrument (Nanoparticle and Nanotechnology Research Center at Institut Teknologi Bandung). The TEM images were also analyzed using ImageJ software to determine the particle size distribution. A Horiba SZ-100 dynamic laser scattering (DLS) instrument (Nanoparticle and Nanotechnology Research Center, Institut Teknologi Bandung) was used to measure the hydrodynamic size of particle. For this measurement, 0.001 g of the nanoparticle specimen was suspended in 10 mL demineralized water and sonicated for 15 minutes. Afterwards, the specimen suspension was analyzed at 633 nm laser wavelength and 173° scattering detector angle.

Antimicrobial Activity Measurement

The antibacterial properties of the biosynthesized ZnO nanoparticles were measured using the microtiter dish biofilm assay method [43, 44]. *Escherischia coli* ATCC 25922 was selected as the model microbe. The bacteria were grown on the surface of solid substrate in the form of biofilm, in which the bacteria are protected by an extracellular polymeric

substance (EPS) secreted by the bacterial colony. Thus, the antibacterial property may be more specifically defined in this case as antibiofilm activity. To prepare the bacterial inoculum, a single colony grown on nutrient agar (NA) medium was selected and added into 5 mL of Luria Bertani (LB) medium containing 10 g/L tryptone, 5 g/L yeast extract, and 10 g/L NaCl and incubated overnight at a temperature of 30 °C and a rotational speed of 150 rpm in an incubator shaker apparatus.

For the antibiofilm assay procedure, 1 mL of the overnight *E. coli* inoculum was mixed with 50 mL M9 minimal salt growth medium containing 48 mM Na₂HPO₄, 22 mM KH₂PO₄, 9 mM NaCl, 19 mM NH₄Cl, 2 mM MgSO₄.7H₂O, 100 μ M CaCl₂ and 20 mM glucose. All chemicals were purchased from Merck and were of analytical grade. The low nutrient availability provided by the M9 medium simulates a nutritionally unfavorable environment for the bacterial colony, thereby inducing their attachment to solid surfaces and the formation of biofilm. A 24-well plate was used for the assay, in which 0.9 mL bacterial suspension aliquot was added to the each well on the plate. Then, 0.1 mL of ZnO nanoparticle suspension was added to each well. The concentration of ZnO in this suspension was varied to produce final ZnO concentrations of 50 and 200 ppm.

The microwell plate was incubated for 4.5 hours at 37 °C, 180 rpm. At the end of incubation, the supernatant in the wells was carefully removed. The biofilm remaining in the internal surfaces of the wells was washed with 1.75 mL phosphate buffered saline (PBS) solution. After the PBS solution was removed, the biofilm was stained by 1 mL of 0.1% crystal violet solution followed by 15 minutes incubation. Afterwards, the excess stain solution was washed off and the residual stain remaining in the biofilm was dissolved in 1.75 mL of analytical grade ethanol followed by analysis using an ultraviolet-visible light (UV-Vis) spectrophotometer. Absorbance or optical density at 570 nm light wavelength (denoted by the OD570 shorthand) was normalized against OD570 of positive control specimen, producing the residual *E. coli* population in the biofilm relative to the initial total bacterial population.

Results

Biosynthesis and Characterization of ZnO Nanoparticles

A simultaneous TGA-DSC instrument was used to evaluate a precipitate specimen that was created in a preliminary experiment at a ratio of 2 and biosynthesis temperature of 60 °C to determine the suitable calcination temperature. The specimen was heated in flowing air to a maximum temperature of 600 °C at a constant rate of 10 °C/min. A strong endothermic thermal event occurred in the range of 370 to 405 °C (Figure 2), resulting in a mass loss of approximately 50%. The burning of organic matter from the bilimbi extract, as well as the thermal decomposition of zinc hydroxide and zinc hydroxynitrate molecules into ZnO, were identified as the causes of this endothermic mass loss event [39, 45]. Based on these results, calcination of raw, dried biosynthesis precipitate was set at 375 °C for 1 hour.

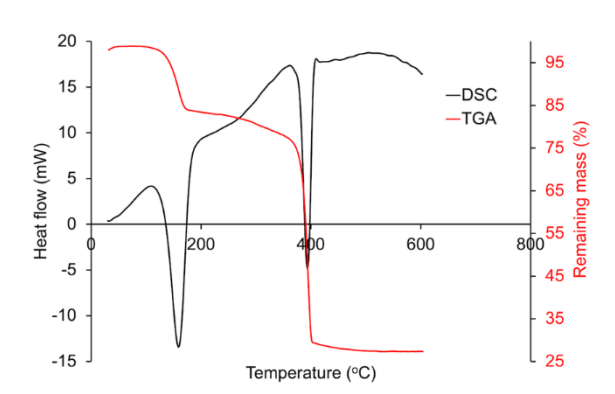


Figure 2 Simultaneous DSC/TGA thermal analyses results of the biosynthesized precipitate specimen from the preliminary experiment heated non-isothermally in flowing air atmosphere at 10 °C/min rate.

To confirm the formation of ZnO, selected specimens of the calcined nanoparticles (synthesized at 60 °C, ratio 0.5, both for physical and chemical deagglomerated methods) were analyzed by XRD (Figure 3). All biosynthesized ZnO exhibited excellent crystallinity overall, with distinct and sharp diffraction peaks. The biosynthesized ZnO specimens exhibited even higher crystallinity than the commercial ZnO. The angles and relative intensities of the diffraction peaks matched the hexagonal wurtzite crystalline ZnO phase [42]. By comparing the results with the commercial ZnO nanoparticle specimen, the prevalence of wurtzite was also confirmed, while the presence of other crystalline phases was negligible. Crystallite sizes determined by the familiar Scherrer equation and degree of crystallinity are summarized in Table 2.

Table 2 ZnO nanoparticle crystallite sizes and degree of crystallinity determined from X-ray diffractograms.

Specimen	Crystal mean diameter (nm)	Degree of crystallinity (%)
Chemical deagglomerated	21.09	82.5%
Physical deagglomerated	17.60	85%
Commercial	28.15	76.4%

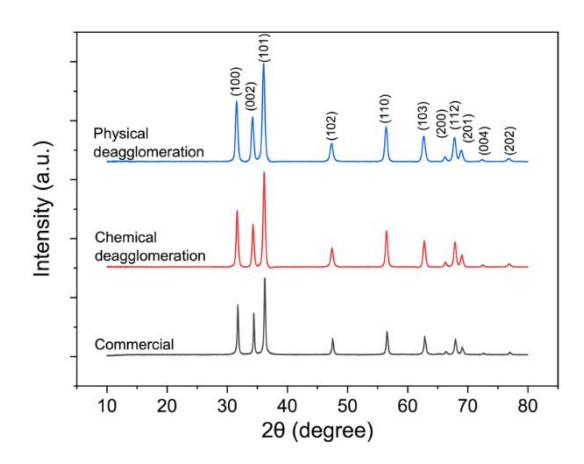


Figure 3 Crystalline phase identification results by XRD of ZnO nanoparticles that was physically deagglomerated (blue lines) and chemically deagglomerated (red lines). XRD spectra of commercial ZnO is also shown. All ZnO specimen were synthesized at 60 °C with a ratio of 0.5.

Transmission electron microscopy images of ZnO nanoparticle specimens and the respective size distribution for single particles are presented (Figure 4). The micrographs reveal well-defined ZnO nanoparticles, characterized by the hexagonal crystal habit typical of the wurtzite phase. Additionally, cuboidal and spherical geometries were observed among the particles. Size measurements indicated that most specimens had diameters ranging from 18 to 27 nm. Larger particles were particularly noticeable in samples synthesized at higher temperature of 60 °C with a ratio of 2, both for chemical (average particle size 28.83 nm) and physical deagglomeration (average particle size 30.74 nm). The average particle size obtained here aligns with previously reported sizes of ZnO nanoparticle biosynthesized using sorghum seed extract (approximately 20-30 nm) [41].

Visual examination of the specimens indicated the absence of particle fusion in all samples, which suggested that only soft agglomerates were formed. The relatively low calcination temperatures used across all samples likely prevented the formation of hard agglomerates, which are typically marked by necking or interparticle bridging and are more common at higher calcination temperatures [46]. Given that only soft agglomerates were observed in all samples with similar nanoparticle sizes, the extent of agglomeration and the effectiveness of deagglomeration were further evaluated by hydrodynamic size distribution, as explained below.

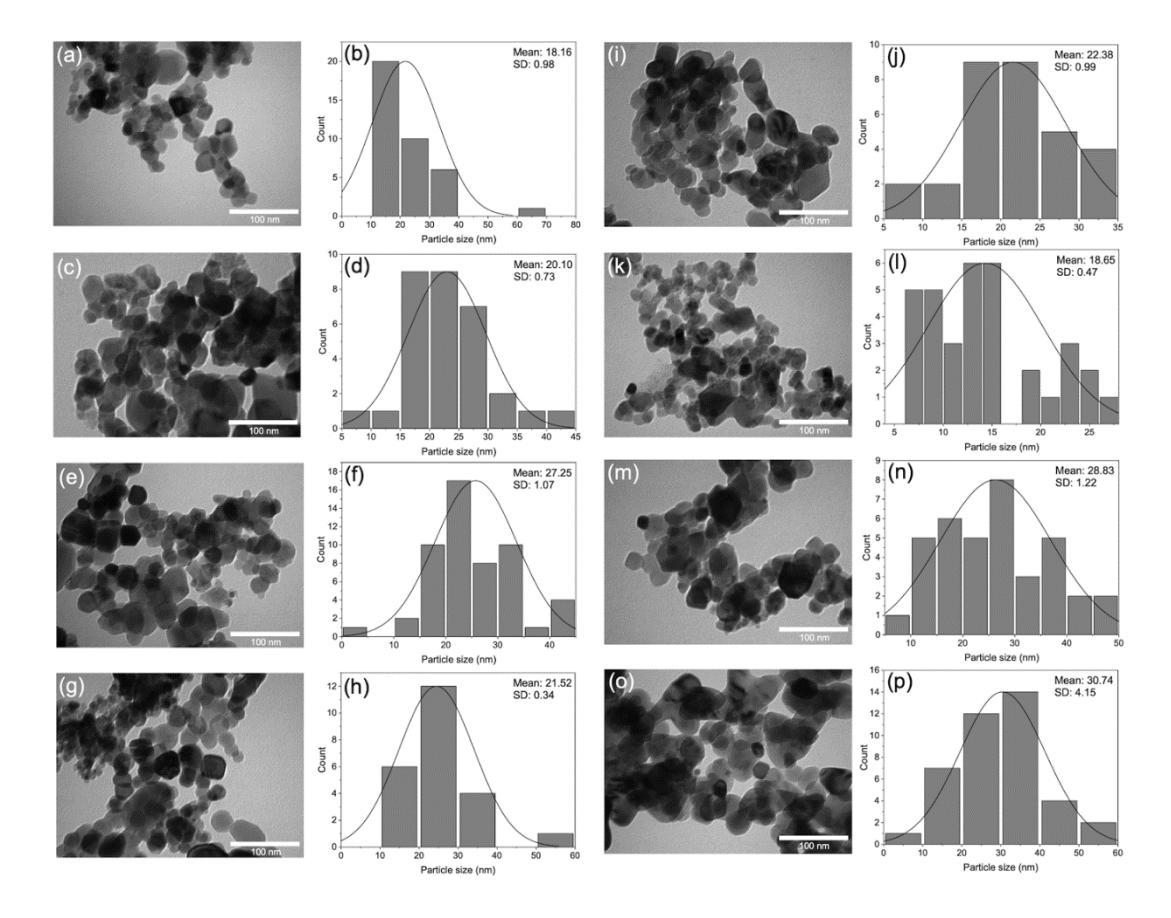


Figure 4 TEM images and corresponding particle size distribution histogram for ZnO specimens synthesized at different conditions: (a,b) chemical deagglomeration, 30 °C, ratio 0.5; (c,d) physical deagglomeration, 30 °C, ratio 0.5; (e,f) chemical deagglomeration, 60 °C, ratio 0.5; (g,h) physical deagglomeration, 60 °C, ratio 0.5; (i,j) chemical deagglomeration, 30 °C, ratio 2; (k,l) physical deagglomeration, 60 °C, ratio 2; (o,p) physical deagglomeration, 60 °C, ratio 2.

Table 3 summarizes the results from the DLS measurements, namely particle mean hydrodynamic diameter and polydispersity index (PDI). The mean hydrodynamic diameters ranged from 1.0 to 3.5 μ m, while PDI values were calculated as 0.88 to 2.96. The smallest hydrodynamic diameter was obtained when the synthesis was performed at 30 °C with a ratio of 0.5 using chemical deagglomeration method. The results of the statistical analysis using ANOVA for a full factorial experiment with replicated runs, in which all main and interaction effects could be calculated and their statistical significances evaluated against a significance level of 0.05, are summarized in Table 4. The regression was limited to binary or two-way interactions, due to the generally unlikely significance of three-way interactions according to the commonly adopted statistical sparsity of effects principle. Both non-adjusted and adjusted coefficients of correlations of the particle hydrodynamic diameter ANOVA data treatment indicated an excellent fit between measurement and computed regression model.

Table 3	Hydrodynamic particle size and PDI results of biosynthesized ZnO.

Deagglomeration method (X ₁)	Synthesis T, °C (X₂)	Precursor:extract ratio (X ₃)	Hydrodynamic mean diameter (nm)	PDI
Chemical	30	0.5	1169	2.96
Physical	30	0.5	3337	1.79
Chemical	60	0.5	2987	1.10
Physical	60	0.5	1494	1.73
Chemical	30	2.0	3093	1.01
Physical	30	2.0	3534	1.12
Chemical	60	2.0	3164	1.00
Physical	60	2.0	3151	0.88

-	Mean hydrody	namic dian	Р	PDI		
Source of variance	Coefficient (coded variables)	F ₀	P- value	Coefficient (coded variables)	F ₀	P- value
X ₁ (Deag. Method)	138.0	20.41	< 0.000	-0.071	1.39	0.255
X ₂ (Synthesis T)	-42.1	1.90	0.187	-0.272	20.76	< 0.000
X₃ (Precursor/extract)	494.4	262.15	< 0.000	-0.447	56.11	< 0.000
X_1X_2	-514.4	283.80	< 0.000	0.196	10.83	0.005
X_1X_3	-31.0	1.03	0.326	0.067	1.24	0.281
X_2X_3	-35.7	1.37	0.259	0.207	12.00	0.003
Coeff. of						
correlation						
R^2	97.89 %			88.27 %		
Adjusted R ²	96.97 %			83.14 %		

 Table 4
 ANOVA data for treatment results of biosynthesized ZnO hydrodynamic particle size.

Antibiofilm Activity Measurements

The antibiofilm activity of ZnO specimens were tested at final concentrations of 50 and 200 ppm against E. coli biofilm. The doses refer to the ZnO nanoparticle mass content within each well. This addition expanded the three-factor complete factorial experiment in Table 1 into a 2^4 full factorial design with ZnO dose as the fourth variable (X4). Table 5 summarizes the antibiofilm activity experimental results. The antibiofilm activity was calculated from the ratio of the residual bacterial population against control (biofilm population without the addition of ZnO). Each antibiofilm activity value in Table 5 was an average of three run replicates.

		•				•	•	
Deagglo- meration method (X ₁)	Biosynthe sis T, °C (X ₂)	Precursor: extract (v/v) (X ₃)	ZnO dose, ppm (X ₄)	Residual biofilm population, %			Antibiofilm activity, %	
				Rep.1	Rep.2	Rep.3	Avg.	
Ch avaisasi	20	0.5	50	16.53	18.60	8.69	14.6	85.4
Chemical	30	0.5	200	11.82	7.38	4.38	7.9	92.1
Dhusiaal	20	0.5	50	14.96	18.60	28.56	20.7	79.3
Physical	30	0.5	200	5.10	5.79	4.18	5.0	95.0
Chamical	60	0.5	50	65.08	51.73	66.69	61.2	38.8
Chemicai	Chemical 60	0.5	200	2.01	29.52	35.16	22.2	77.8
Dhysical	ysical 60 0.5	0.5	50	53.75	27.71	61.06	47.5	52.5
Physical		0.5	200	21.19	6.47	32.98	20.2	79.8
Chemical	30	2	50	47.18	42.62	29.69	39.8	60.2
Chemicai	30	2	200	5.60	11.30	30.17	15.7	86.2
Physical	30	2	50	24.72	7.11	34.43	22.1	77.9
Pilysical	Physical 30	2	200	34.67	18.05	33.71	28.8	71.2
Chemical	60	2	50	64.69	42.71	66.45	58.0	42.0
Chemical	OU	۷	200	42.32	28.21	32.94	34.5	65.5
Dhysical	60	2	50	62.82	41.43	45.37	49.9	50.1
Physical 60	2	200	47.13	42.56	29.63	39.8	60.2	

Table 5 Factorial experimental matrix and antibiofilm activity data of biosynthesized ZnO.

The residual *E. coli* population values after 4.5 hours of incubation produced by the experimental design matrix in Table 4 are presented in Figure 5. At a nanoparticle dose of 50 ppm, the between-run average antibactivity was 61%. As the dose was increased to 200 ppm, the average antibiofilm activity reached 78%. The highest activity measured in all runs was 95%, obtained by biosynthesized ZnO that was physically deagglomerated and synthesized at 30 °C and ratio of 0.5.

Summary of the ANOVA treatment of the antibiofilm activity data is presented in Table 6. By invoking the sparsity of effect principle, the interaction effect of the highest order interaction (in this case the four-way interaction) was dropped from the analysis. At 95% confidence level, all three-way interactions were found to not be significant. Only one interaction was in fact significant, namely that between biosynthesis temperature and nanoparticle dose (X_2X_4) . A series of model refinement was undertaken, resulting in the elimination of all three- and two-way interactions except X_2X_4 . Table 7 presents the ANOVA results using the final model. All terms remaining after the model refinement were statistically significant at 95% confidence level.

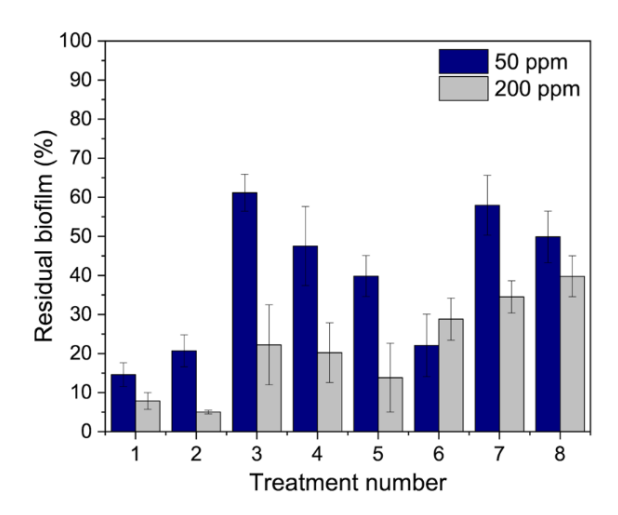


Figure 5 Residual biofilm population of *E. coli* in systems containing biosynthesized ZnO nanoparticles at final concentrations of 50 and 200 ppm. The residual bacterial population denotes the OD570 of biofilm in each well normalized by the OD570 value of control (without ZnO addition). The error bar indicates the standard error between the triplicates.

Table 6 ANOVA data treatment of the residual biofilm population after 4.5 hrs of contact with biosynthesized ZnO nanoparticles at 50 and 200 ppm doses.

Source of variance	Coefficient (coded variables)	F_0	P-value	Standardized effect
X ₁ (Deag. Method)	-1.24	0.61	0.439	0.783
X ₂ (Biosynth. T)	11.16	49.77	< 0.001	7.055
X ₃ (Precursor:Extract)	5.57	12.41	0.001	3.523
X_4 (ZnO dose)	-8.73	30.43	< 0.001	5.516
X_1X_2	-1.07	0.46	0.504	0.676
X_1X_3	0.31	0.04	0.845	0.197
X_1X_4	2.93	3.44	0.073	1.854
X_2X_3	-1.70	1.16	0.290	1.076
X_2X_4	-3.75	5.61	0.024	2.368
X_3X_4	2.36	2.22	0.146	1.489
$X_1X_2X_3$	1.30	0.67	0.418	0.820
$X_1X_2X_4$	0.19	0.01	0.904	0.122
$X_1X_3X_4$	2.59	2.69	0.111	1.640
$X_2X_3X_4$	1.73	1.19	0.283	1.092
Coeff. of correlation				
R^2	77.93 %			
R^2_{adj}	67.58 %			

 Table 7
 ANOVA data treatment summary of residual biofilm population after model refinement.

Source of variance	Coefficient (coded variables)	F_0	P-value
X ₂ (Biosynthesis T, °C)	11.16	47.24	< 0.001
X ₃ (Precursor:extract, v/v)	5.57	11.06	0.002
X ₄ (Nanoparticle dose, ppm)	-8.73	29.05	< 0.001
X ₂ *X ₄	-3.75	4.89	0.028
R ²	67.75 %		
R^2_{adj}	64.75 %		

The precursor:extract ratio (X₃) exhibited a positive regression coefficient, implying that the *E. coli* antibiofilm activity was improved by adding more bilimbi extract (in this case by increasing the volumetric proportion of the bilimbi extract, at constant extract concentration) to the reacting system. A similar behavior was reported by Skandalis *et al.* [47], who argued that higher quantities of biomolecules present in the reacting system imply a higher availability of capping agents. This in turn limits the particle growth as the biosynthesis proceeds.

The two-way interactions between biosynthesis and deagglomeration experimental variables are described by the interaction plot in Figure 6.

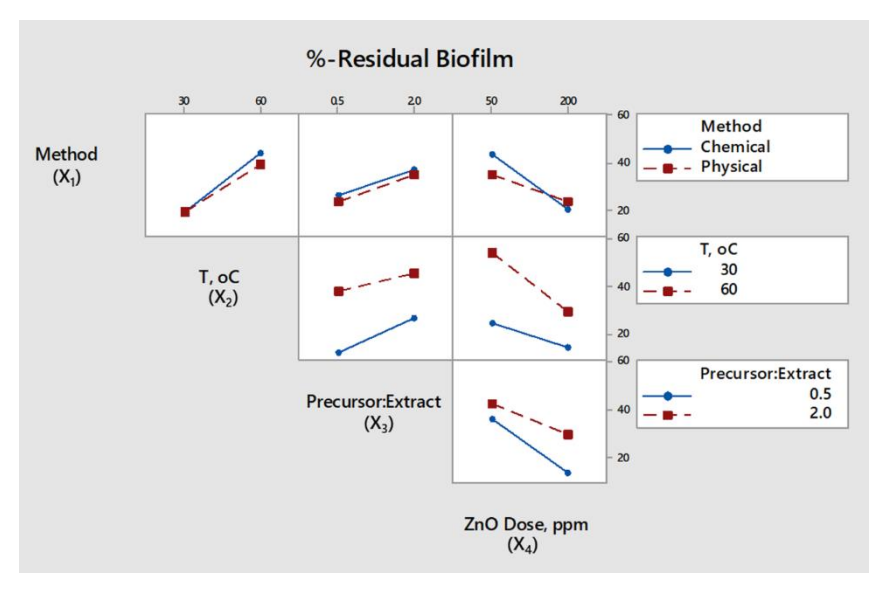


Figure 6 Interaction effects between ZnO biosynthesis variables on the antibiofilm activity.

Numbers along the vertical axis represent the antibiofilm activity as percentage of the residual biofilm populations, averaged across the triplicate runs. Of the six two-way interactions, the one between biosynthesis temperature and nanoparticle dose (X_2X_4) exhibited the largest difference between the slope of the paired curves. The slopes of the X_2X_4 interaction pair imply that higher activity (or lower residual *E. coli* population) may be achieved by combining lower biosynthesis temperature and higher nanoparticle dose. The presence of this two-way interaction suggested that the effect on antibiofilm activity should be larger than if either biosynthesis temperature or ZnO dose was varied individually.

Discussion

Biosynthesis and Characterization of ZnO Nanoparticles

The ANOVA data treatment results for biosyntesized ZnO nanoparticles size in Table 4 indicate that not all effects significantly influenced the mean particle hydrodynamic diameter. The main effects of the deagglomeration method (X_1) and ratio (X_3) were highly significant (p-value < 0.000). The regression coefficient of X_1 was positive, implying that a change from chemical to physical deagglomeration method increases the particle size. The coefficient of X_3 was positive as well, indicating that shifting to a higher ratio in the reaction mixture increases the particle size. As a comparison, Skandalis *et al.* [47] observed a reduction in particle diameters from 50-60 nm to 40 nm when the volume of plant extract in the biosynthesis reaction mixture was doubled. At lower extract volume (or concentration), the reduction rate of Z_1^{2+} was slower. This slower reduction rate allows more time for particle agglomerates to form and grow. The binary interaction between deagglomeration method and biosynthesis temperature (X_1X_2) was also found to be significant. Regression coefficient of X_1X_2 was negative, which suggests that a smaller particle size may be attained by the simultaneous selection of chemical deagglomeration (lower or 'negative' level of X_1 in the design matrix) and lowering the biosynthesis temperature (also lower or 'negative' level of X_2 , thus producing a positive multiplication product of X_1 and X_2).

DOI: 10.5614/j.eng.technol.sci.2024.56.6.5

When the focus was placed on physical deagglomeration by ultrasonication, the negative coefficient of X_1X_2 interaction implied that the effectiveness of ultrasonication in breaking the agglomerates was more pronounced at higher temperature. This was observed by the mean agglomerate hydrodynamic diameters of 2.5-4.5 μ m at 50 °C, which was reduced to 1.5-3.0 μ m when the biosynthesis/deagglomeration temperature was raised to 70 °C. This trend was likely due to the increase in nanoparticle salt precursor solubility with temperature, which shifted the reaction equilibrium away from the supersaturation of the salt. This shift then delayed the formation of agglomerates. In addition to the temperature effect, increasing the zinc precursor concentration in biosynthesis combined with concurrent ultrasonication could increase the diameter of the nanoparticle product [48].

An analogous interaction interpretation of chemical deagglomeration suggests that using PVA as deagglomerant was more effective at lower biosynthesis temperature. The acetate groups in PVA molecules tend to ionize at lower pH values. It has been reported that in systems containing oxide nanoparticles under acidic condition (pH = 3), the negatively charged acetate groups electrostatically bond with hydrolyzed metal cations on the nanoparticle surface. When pH is increased to nearly neutral (pH = 6), the degree of acetate group ionization is also decreased, resulting in a decrease of PVA molecule adsorption on the nanoparticle surface [49]. In this research, elevating the biosynthesis temperature in chemical deagglomeration increased the nanoparticle agglomerate size. This was likely due to the point of zero charge (PZC) of ZnO, which occurs in a pH range of 8.0-9.0, while the bilimbi extract used in the biosynthesis resulted in a much more acidic condition (pH \sim 2.5). The strong electrostatic attraction between the positively charged oxide nanoparticle surface and the negatively charged ionized acetate groups in the PVA is believed to cause the PVA molecules to curl. This curling reduces the layer of PVA adsorbed on the nanoparticle surface. A higher temperature promotes acetate ionization, further diminishing the PVA adsorption layer, which effectively reduces the interparticle steric hindrance necessary for deagglomeration [50, 51].

The effect of the deagglomeration and biosynthesis conditions was also assessed based on the ANOVA treatment of measured PDI values in Table 3. The literature suggest that a monodispersed or uniformly sized nanoparticle system should exhibit a PDI of 0.1 to 0.25. In contrast, a PDI above 0.7 generally suggests a polydispersed or non-uniformly sized system [52]. Based on these criteria, the specimens in this research exhibited agglomeration, which was consistent with visual observation by TEM and the micron-level mean particle hydrodynamic diameters measured by DLS. Statistical analysis identified synthesis temperature (X_2) and precursor:extract ratio (X_3) as significant variables, while deagglomeration method did not significantly alter the PDI. Regression coefficients of both X_2 and X_3 were negative, implying that narrower particle size distribution (indicated by decreased PDI) was achieved by individually selecting a higher synthesis temperature and a higher proportion of precursor quantity in the reacting system. However, since binary interactions X_1X_2 and X_2X_3 were also statistically significant, at a 95% confidence level, selection of all three biosynthesis variables cannot be undertaken individually.

The positive X_1X_2 coefficient suggests that a narrower particle size distribution may be obtained by either selecting a combination of chemical deagglomeration and higher temperature, or physical deagglomeration at a lower temperature. Analogously, the positive X_2X_3 coefficient implies that lower PDI may be obtained by selecting a combination of a lower temperature and a higher precursor:extract ratio, or a higher temperature and a lower precursor:extract ratio. The coefficients of correlation for the ANOVA treatment of PDI data in Table 4 suggest a good fit of the measured data with the regression model.

Antibiofilm Activity Measurement

The antibiofilm activities in Table 5 are comparable to results reported in the literature that used a similar biofilm assay protocol. For instance, Husain *et al.* [53] reported a 65% reduction in *E. coli* biofilm formation using ZnO nanoparticles synthesized with *Plumbago zeylanica* root extract at a 100 ppm dosage. Similarly, Doğan and Kocabaş [54] observed a 35% reduction in *E. coli* biofilm using 50 ppm of ZnO prepared from *Veronica multifida* leaf extract. Compared to the antibiofilm activity of commercially available ZnO nanoparticles reported in an earlier study [18], the biosynthesized ZnO nanoparticles in the present work demonstrated higher antibiofilm activity (61% vs. 32% reduction at 50 ppm ZnO, and 78% vs. 40% reduction at 200 ppm ZnO, respectively). This shows the enhanced antibiofilm efficacy of the biosynthesized ZnO nanoparticles over their commercial counterparts. As indicated by XRD analysis, the biosynthesized ZnO typically featured smaller nanoparticle diameters and higher crystallinity, which are factors known to significantly enhance the antibacterial and antibiofilm effectiveness of ZnO nanoparticles. Generally, smaller nanoparticles and higher crystallinity correlate with increased nanoparticle toxicity [13, 20].

Table 7 provides some insight in the antibiofilm activity behavior of the biosynthesized ZnO, as influenced by the deagglomeration method applied during the synthesis process. Signs of the main effects suggest the direction by which the levels of each experimental variable should be set individually. In this context, the activity against *E. coli* biofilm may be increased at a lower biosynthesis temperature, a higher proportion of bilimbi extract relative to the Zn salt precursor solution, and a higher dose of biosynthesized nanoparticles in contact with the biofilm colony. Deagglomeration method selection was not identified as significant in and of itself in Table 6, although the ANOVA results of particle size distribution data in Table 4 indicate that this variable did significantly impact the agglomeration of biosynthesized ZnO.

An increase in ZnO nanoparticle size with biosynthesis temperature has also been reported in the literature [55, 56]. Aside from increased Zn cation dissolution, smaller nanoparticles also offer a larger specific surface area to which the various moeites associated with biomolecules in the plant extract may attach themselves. These biomolecules themselves could exhibit antimicrobial properties, so their presence on the nanoparticle surface further enhances the antimicrobial activity of the nanoparticles [57]. A thorough investigation into the mechanism of action of biosynthesized ZnO and the role of biomolecules in their antimicrobial activity are key challenges that could be addressed in future research.

Conclusions

Zinc oxide nanoparticles in the hexagonal wurtzite structure with high phase purity was produced via a biosynthesis method using *Averrhoa bilimbi* fruit extract combined with physical or chemical deagglomeration techniques. Soft agglomerates were still observable after deagglomeration techniques were conducted. Laser scattering measured mean hydrodynamic diameters of the agglomerates in the 1.2-3.5 µm range and PDI values between 0.88 and 2.96. By employing PVA and a lower precursor-to-extract ratio during chemical deagglomeration, a finer ZnO agglomerate was produced. Physical deagglomeration was more effective at higher temperatures, but chemical deagglomeration was more efficient at lower temperatures, according to a statistically significant interaction between the deagglomeration method and biosynthesis temperature. At 50 ppm dosage, the average activity of biosynthesized ZnO nanoparticle against *E. coli* biofilm was 61%; at a dosage of 200 ppm, this antibiofilm activity increased to 78%. The antibiofilm action was enhanced by increasing the amount of bilimbi extract during the biosynthesis to provide a higher availability of reducing and capping agents. A lower biosynthesis temperature was also indicated to increase antibiofilm activity related to the decreased biomolecular breakdown as the synthesis proceeded.

Data Availability

The authors hereby attest that all images and measurement data that support the findings and conclusions of this work are included in the paper. Upon reasonable request, the corresponding author may supply raw data in other formats if necessary.

Acknowledgments

Institut Teknologi Bandung has provided financial support for this research by the Research, Community Empowerment, and Innovation Program (PPMI ITB). The funding was granted on behalf of the Sustainable Chemical Engineering Product Research Group of the Faculty of Industrial Technology.

Compliance with ethics guidelines

The authors declare that they have no conflict of interest or financial conflicts to disclose.

This article does not contain any studies with human or animal subjects performed by any of the authors.

References

[1] Tiwari, J.N., Tiwari, R.N. & Kim, K.S., Zero-dimensional, One-dimensional, Two-dimensional and Three-dimensional Nanostructured Materials for Advanced Electrochemical Energy Devices, Prog Mater Sci, **57**, pp. 724-803, 2012. doi: 10.1016/j.pmatsci.2011.08.003.

- [2] Naahidi, S., Jafari, M., Edalat, F., Raymond, K., Khademhosseini, A. & Chen, P., *Biocompatibility of Engineered Nanoparticles for Drug Delivery*, J Control Release, **166**, pp. 182-194, 2013. doi: 10.1016/j.jconrel.2012.12.013.
- [3] McNamara, K. & Tofail, S.A.M., *Nanoparticles in Biomedical Applications*, Adv Phys X, **2**, pp. 54-88, 2017. doi: 10.1080/23746149.2016.1254570.
- [4] Jiao, M., Zhang, P., Meng, J., Li, Y., Liu, C., Luo, X. & Gao, M., Recent Advancements in Biocompatible Inorganic Nanoparticles Towards Biomedical Applications, Biomater Sci, 6, pp. 726-745, 2018. doi: 10.1039/c7bm01020f.
- [5] Nikolova, M.P. & Chavali, M.S., *Metal Oxide Nanoparticles as Biomedical Materials*, Biomimetics, **5**, 5020027, 2020. doi: 10.3390/BIOMIMETICS5020027.
- [6] Kielbik, P., Kaszewski, J., Rosowska, J., Wolska, E., Witkowski, B.S., Gralak, M.A., Gajewski, Z., Godlewski, M. & Godlewski, M.M., *Biodegradation of the ZnO:Eu Nanoparticles in the Tissues of Adult Mouse after Alimentary Application*, Nanomedicine, **13**, pp. 843-852, 2017. doi: 10.1016/j.nano.2016.11.002.
- [7] Jiang, J., Pi, J. & Cai, J., *The Advancing of Zinc Oxide Nanoparticles for Biomedical Applications*, Bioinorg Chem Appl, **2018**, 1062562, 2018. doi: 10.1155/2018/1062562.
- [8] Manojkumar, K., Sivaramakrishna, A. & Vijayakrishna, K., A Short Review on Stable Metal Nanoparticles Using Ionic Liquids, Supported Ionic Liquids, and Poly(Ionic Liquids), J Nanopart Res, 18, pp. 1-22, 2016. doi: 10.1007/s11051-016-3409-y.
- [9] Parihar, V., Raja, M. & Paulose, R., A Brief Review of Structural, Electrical and Electrochemical Properties of Zinc Oxide Nanoparticles, Rev Adv Mater Sci, **53**, pp. 119-130, 2018. doi: 10.1515/rams-2018-0009.
- [10] Mandal, A.K., Katuwal, S., Tettey, F., Gupta, A., Bhattarai, S., Jaisi, S., Bhandari, D.P., Shah, A.K., Bhattarai, N. & Parajuli, N., *Current Research on Zinc Oxide Nanoparticles: Synthesis, Characterization, and Biomedical Applications*, Nanomaterials, **12**, 3066, 2022. doi: 10.3390/nano12173066.
- [11] Reda, A.T., Park, J.Y. & Park, Y.T., *Zinc Oxide-based Nanomaterials for Microbiostatic Activities: A Review*, J Funct Biomater, **15**, 103, 2024. doi: 10.3390/jfb15040103.
- [12] Krishnamoorthy, R., Athinarayanan, J., Periyasamy, V.S., Alshuniaber, M.A., Alshammari, G., Hakeem, M.J., Ahmed, M.A. & Alshatwi, A.A., *Antibacterial Mechanisms of Zinc Oxide Nanoparticle against Bacterial Food Pathogens Resistant to Beta-lactam Antibiotics*, Molecules, **27**, 2489 pp. 1-17, 2022. doi: 10.3390/molecules27082489
- [13] Siddiqi, K.S., ur Rahman, A., Tajuddin & Husen, A., *Properties of Zinc Oxide Nanoparticles and Their Activity Against Microbes*, Nanoscale Res Lett, **13**, 141, 2018. doi: 10.1186/s11671-018-2532-3.
- [14] Wang, L., Hu, C. & Shao, L., *The Antimicrobial Activity of Nanoparticles: Present Situation and Prospects for the Future*, Int J Nanomedicine, **12**, pp. 1227-1249, 2017. doi: 10.2147/IJN.S121956.
- [15] Raghunath, A. & Perumal, E., *Metal Oxide Nanoparticles as Antimicrobial Agents: A Promise for the Future*, Int J Antimicrob Agents, **49**, pp. 137–152, 2017. doi: 10.1016/j.ijantimicag.2016.11.011.
- [16] Wang, Y., Liu, J., Wang, T., Liu, L.Z., Tian, C., Cui, Y., Shao, W., Hua, X., Shi, Y. & Wang, Y., *Antibacterial Properties and Mechanism of Nanometer Zinc Oxide Composites*, Food Packag Shelf Life, **40**, 101167, 2023. doi: 10.1016/j.fpsl.2023.101167.
- [17] Sajjad, S., Leghari, S.A.K., Ryma, N.A. & Farooqi, S.A., *Green Synthesis of Metal-based Nanoparticles and Their Applications, Green Metal Nanoparticles: Synthesis, Characterization, and Their Applications*, edited by Kanchi, S. & Ahmed, S., Hoboken: Wiley, pp. 23-54, 2018. doi: 10.1002/9781119418900.ch2.
- [18] Rahayu, E., Wonoputri, V. & Samadhi, T.W., *Plant Extract-assisted Biosynthesis of Zinc Oxide Nanoparticles and Their Antibacterial Application*, IOP Conf Ser Mater Sci Eng, **823**, 012036, 2020. doi: 10.1088/1757-899X/823/1/012036.
- [19] Rasool, A., Kanagaraj, T., Mir, M.I., Zulfajri, M., Ponnusamy, V.K. & Mahboob, M., *Green Coalescence of CuO Nanospheres for Efficient Anti-microbial and Anti-cancer Conceivable Activity*, Biochem Eng J, **187**, 108464, 2022. doi: 10.1016/j.bej.2022.108464.
- [20] Wonoputri, V., Wijaya, J., Primayudha, V.A., Khairunnisa, S. & Samadhi, T.W., *Performance of Antimicrobial ZnO Nanoparticle Synthesized by Biological Method: Literature Review*, AIP Conf Proc, **2667**, 050007, 2023. doi: 10.1063/5.0118678.
- [21] Al-darwesh, M.Y., Ibrahim, S.S. & Mohammed, M.A., *A Review on Plant Extract Mediated Green Synthesis of Zinc Oxide Nanoparticles and Their Biomedical Applications*, Results Chem, **7**, 101368, 2024, doi: 10.1016/j.rechem.2024.101368.
- [22] Suluvoy, J.K. & Berlin Grace, V.M., *Phytochemical Profile and Free Radical Nitric Oxide (NO) Scavenging Activity of Averrhoa Bilimbi L. Fruit Extract*, 3 Biotech, **7**, 85, 2017. doi: 10.1007/s13205-017-0678-9.

- [23] Rahman, M.M., Habib, M.R., Hasan, M.A., Amin, M.Al, Saha, A. & Mannan, A., Comparative Assessment on in Vitro Antioxidant Activities of Ethanol Extracts of Averrhoa Bilimbi, Gymnema Sylvestre and Capsicum Frutescens, Pharmacognosy Res, 6, pp. 36-41, 2014. doi: 10.1007/s00289-017-2025-z.
- [24] Utami, S., Endrini, S., Nafik, S., Lestari, I.M.T., Anindya, D., Bakar, E.A., Rozy, F., Said, F.F., Afifah, E., Arumwardana, S., Nufus, H., Rihibiha, D.D., Kusuma, H.S.W., Wibowo, S.H.B. & Widowati, W., *In Vitro Antioxidant and Antiobesity Activities of Freeze-dried Canarium Sp., Averrhoa Bilimbi L. and Malus Domestica*, Indones Biomed J, **11**, pp. 320-326, 2019. doi: 10.18585/inabj.v11i3.728.
- [25] Yan, S.W., Ramasamy, R., Alitheen, N.B.M. & Rahmat, A., A Comparative Assessment of Nutritional Composition, Total Phenolic, Total Flavonoid, Antioxidant Capacity, and Antioxidant Vitamins of Two Types of Malaysian Underutilized Fruits (Averrhoa bilimbi and Averrhoa carambola), Int J Food Prop, 16, pp. 1231-1244, 2013. doi: 10.1080/10942912.2011.582975.
- [26] Khairunnisa, S., Wonoputri, V. & Samadhi, T.W., Effective Deagglomeration in Biosynthesized Nanoparticles: A Mini Review, IOP Conf Ser Mater Sci Eng, 1143, 012006, 2021. doi: 10.1088/1757-899x/1143/1/012006.
- [27] Liu, Y.S., Chang, Y.C. & Chen, H.H., Silver Nanoparticle Biosynthesis by Using Phenolic Acids in Rice Husk Extract as Reducing Agents and Dispersants, J Food Drug Anal, **26**, pp. 649-656, 2018. doi: 10.1016/j.jfda.2017.07.005.
- [28] Cao, X., Zhu, L., Bai, Y., Li, F. & Yu, X., *Green One-step Synthesis of Silver Nanoparticles and Their Biosafety and Antibacterial Properties*, Green Chem Lett Rev, **15**, pp. 28-34, 2022. doi: 10.1080/17518253.2021.2018506.
- [29] Aminuzzaman, M., Ying, L.P., Goh, W.S. & Watanabe, A., *Green Synthesis of Zinc Oxide Nanoparticles Using Aqueous Extract of Garcinia Mangostana Fruit Pericarp and Their Photocatalytic Activity*, B Mater Sci, **41**, 50, 2018. doi: 10.1007/s12034-018-1568-4.
- [30] Shanavas, S., Priyadharsan, A., Karthikeyan, S., Dharmaboopathi, K., Ragavan, I., Vidya, C., Acevedo, R. & Anbarasana, P.M., *Green Synthesis of Titanium Dioxide Nanoparticles Using Phyllanthus Niruri Leaf Extract and Study on Its Structural, Optical and Morphological Properties*, Mater Today Proc, **26**, pp. 3531-3534, 2019. doi: 10.1016/j.matpr.2019.06.715.
- [31] Abdullah, J.A.A., Salah Eddine, L., Abderrhmane, B., Alonso-González, M., Guerrero, A. & Romero, A., *Green Synthesis and Characterization of Iron Oxide Nanoparticles by Pheonix Dactylifera Leaf Extract and Evaluation of Their Antioxidant Activity*, Sustain Chem Pharm, **17**, 100280, 2020. doi: 10.1016/j.scp.2020.100280.
- [32] Droepenu, E.K., Asare, E.A., Wee, B.S., Wahi, R.B., Ayertey, F. & Kyene, M.O., *Biosynthesis, Characterization, and Antibacterial Activity of ZnO Nanoaggregates Using Aqueous Extract from Anacardium Occidentale Leaf: Comparative Study of Different Precursors*, Beni Suef Univ J Basic Appl Sci, **10**, pp. 1-10, 2021.
- [33] Rokbani, H., Daigle, F. & Ajji, A., Combined Effect of Ultrasound Stimulations and Autoclaving on the Enhancement of Antibacterial Activity of ZnO and SiO₂/ZnO Nanoparticles, Nanomaterials, **8**, 129, 2018. doi: 10.3390/nano8030129.
- [34] Pradhan, S., Hedberg, J., Blomberg, E., Wold, S. & Odnevall Wallinder, I., *Effect of Sonication on Particle Dispersion, Administered Dose and Metal Release of Non-functionalized, Non-inert Metal Nanoparticles*, J Nanopart Res, **18**, pp. 1-14, 2016. doi: 10.1007/s11051-016-3597-5.
- [35] Hartmann, N.B., Jensen, K.A., Baun, A., Rasmussen, K., Rauscher, H., Tantra, R., Cupi, D., Gilliland, D., Pianella, F. & Riego Sintes, J.M., *Techniques and Protocols for Dispersing Nanoparticle Powders in Aqueous Media Is There a Rationale for Harmonization?*, J Toxicol Environ Health B Crit Rev, **18**, pp. 1-28, 2015. doi: 10.1080/10937404.2015.1074969.
- [36] Othman, S.H., Abdul Rashid, S., Mohd Ghazi, T.I. & Abdullah, N., *Dispersion and Stabilization of Photocatalytic TiO₂ Nanoparticles in Aqueous Suspension for Coatings Applications*, J Nanomater, **2012**, 71812, 2012. doi: 10.1155/2012/718214.
- [37] Thonglerth, P., Sujaridworakun, P. & Boondamnoen, O., *Preparation of ZnO Nanoparticles Water-based Dispersion*, J Phys Conf Ser, **2175**, 012029, 2022. doi: 10.1088/1742-6596/2175/1/012029.
- [38] Tuok, L.P., Elkady, M., Zkria, A., Yoshitake, T. & Nour Eldemerdash, U., *Evaluation of Stability and Functionality of Zinc Oxide Nanofluids for Enhanced Oil Recovery*, Micro Nano Syst Lett, **11**, 12, 2023. doi: 10.1186/s40486-023-00180-7.
- [39] Mayedwa, N., Khalil, A.T., Mongwaketsi, N., Matinise, N., Shinwari, Z.K. & Maaza, M., *The Study of Structural, Physical and Electrochemical Activity of Zno Nanoparticles Synthesized by Green Natural Extracts of Sageretia Thea*, Nano Research & Applications, **3**, 9, 2017. doi: 10.21767/2471-9838.100026.
- [40] Pallela, P.N.V.K., Ruddaraju, L.K., Veerla, S.C., Matangi, R., Kollu, P., Ummey, S. & Pammi, S.V.N., *Synergetic Antibacterial Potential, Dye Degrading Capability and Biocompatibility of Asperagus Racemosus Root Assisted ZnO Nanoparticles*, Mater Today Commun, **25**(February), 101574, 2020. doi: 10.1016/j.mtcomm.2020.101574.

- [41] Rakgotho, T., Ndou, N., Mulaudzi, T., Iwuoha, E., Mayedwa, N. & Ajayi, R.F., *Green-synthesized Zinc Oxide Nanoparticles Mitigate Salt Stress in Sorghum Bicolor*, Agriculture, **12**, 597, 2022. doi: 10.3390/agriculture12050597.
- [42] Yadav, M.S., Singh, N. & Bobade, S.M., Zinc Oxide Nanoparticles and Activated Charcoal-based Nanocomposite Electrode for Supercapacitor Application, Ionics (Kiel), **24**, pp. 3611-3630, 2018. doi: 10.1007/s11581-018-2527-1.
- [43] Wonoputri, V., Gunawan, C., Liu, S., Barraud, N., Yee, L.H., Lim, M. & Amal, R., Ferrous Ion as a Reducing Agent in the Generation of Antibiofilm Nitric Oxide from a Copper-based Catalytic System, Nitric Oxide, **75**, pp. 8-15, 2018. doi: 10.1016/j.niox.2018.01.005.
- [44] O'Toole, G.A., Microtiter Dish Biofilm Formation Assay, J Vis Exp, 47, 2437, 2011. doi: 10.3791/2437.
- [45] Malucelli, L.C., Massulo, T., Magalhães, W.L.E., Stofella, N.C.F., Vasconcelos, E.C., Filho, M.A.S.C. & Murakami, F.S., *Thermal and Chemical Characterization of Dicksonia Sellowiana Extract by Means of Thermal Analysis*, Rev Bras Farmacogn, **28**, pp. 626-630, 2018. doi: 10.1016/j.bjp.2018.07.001.
- [46] Yeap, S.P., Permanent Agglomerates in Powdered Nanoparticles: Formation and Future Prospects, Powder Technol, **323**, pp. 51-59, 2018. doi: 10.1016/j.powtec.2017.09.042.
- [47] Skandalis, N., Dimopoulou, A., Georgopoulou, A., Gallios, N., Papadopoulos, D., Tsipas, D., Theologidis, I., Michailidis, N. & Chatzinikolaidou, M., *The Effect of Silver Nanoparticles Size, Produced Using Plant Extract from Arbutus Unedo on Their Antibacterial Efficacy*, Nanomaterials, **7**, 178. 2017.doi: 10.3390/nano7070178.
- [48] Tran, Q.M.T., Nguyen, H.A.T., Doan, V.D., Tran, Q.H. & Nguyen, V.C., Biosynthesis of Zinc Oxide Nanoparticles Using Aqueous Piper Betle Leaf Extract and Its Application in Surgical Sutures, J Nanomater, **2021**, 8833864, 2021. doi: 10.1155/2021/8833864.
- [49] Wiśniewska, M., Ostolska, I., Szewczuk-Karpisz, K., Chibowski, S., Terpiłowski, K., Gun'ko, V.M. & Zarko, V.I., Investigation of the Polyvinyl Alcohol Stabilization Mechanism and Adsorption Properties on the Surface of Ternary Mixed Nanooxide AST 50 (Al₂O₃—SiO₂—TiO₂), Journal of Nanoparticle Research, 17, 12, 2015. doi: 10.1007/s11051-014-2831-2.
- [50] Alias, S.S., Ismail, A.B. & Mohamad, A.A., Effect of pH on ZnO Nanoparticle Properties Synthesized by Sol-gel Centrifugation, J Alloys Compd, 499, pp. 231-237, 2010. doi: 10.1016/j.jallcom.2010.03.174.
- [51] Wiśniewska, M., *Temperature Effects on the Adsorption of Polyvinyl Alcohol on Silica*, Central European Journal of Chemistry, **10**, pp. 1236-1244, 2012. doi: 10.2478/s11532-012-0044-z.
- [52] Eftekhari, A., Ahmadian, E., Panahi-Azar, V., Hosseini, H., Tabibiazar, M. & Maleki Dizaj, S., Hepatoprotective and Free Radical Scavenging Actions of Quercetin Nanoparticles on Aflatoxin B1-Induced Liver Damage: In Vitro/in Vivo Studies, Artif Cells Nanomed Biotechnol, 46, pp. 411-420, 2018. doi: 10.1080/21691401.2017.1315427.
- [53] Husain, F.M., Qais, F.A., Ahmad, I., Hakeem, M.J., Baig, M.H., Khan, J.M. & Al-Shabib, N.A., *Biosynthesized Zinc Oxide Nanoparticles Disrupt Established Biofilms of Pathogenic Bacteria*, Appl Sci, **12**, 710, 2022. doi: 10.3390/app12020710.
- [54] Doğan, S.Ş. & Kocabaş, A., *Green Synthesis of ZnO Nanoparticles with Veronica Multifida and Their Antibiofilm Activity*, Hum Exp Toxicol, **39**, pp. 319-327, 2020. doi: 10.1177/0960327119888270.
- [55] Mohammadi, F.M. & Ghasemi, N., Influence of Temperature and Concentration on Biosynthesis and Characterization of Zinc Oxide Nanoparticles Using Cherry Extract, J Nanostructure Chem, **8**, pp. 93-102, 2018. doi: 10.1007/s40097-018-0257-6.
- [56] Basri, H.H., Talib, R.A., Sukor, R., Othman, S.H. & Ariffin, H., Effect of Synthesis Temperature on the Size of ZnO Nanoparticles Derived from Pineapple Peel Extract and Antibacterial Activity of ZnO-starch Nanocomposite Films, Nanomaterials, 10, 1061, 2020. doi: 10.3390/nano10061061.
- [57] Deshmukh, A.R., Gupta, A. & Kim, B.S., 2019, Ultrasound Assisted Green Synthesis of Silver and Iron Oxide Nanoparticles Using Fenugreek Seed Extract and Their Enhanced Antibacterial and Antioxidant Activities, Biomed Res Int, 2019, 1714358, 2019. doi: 10.1155/2019/1714358.